Author/s:
Lei, P;Ayton, S;Appukuttan, AT;Volitakis, I;Adlard, PA;Finkelstein, DI;Bush, AI

Title:
Clioquinol rescues Parkinsonism and dementia phenotypes of the tau knockout mouse

Date:
2015-09-01

Citation:
Lei, P., Ayton, S., Appukuttan, A. T., Volitakis, I., Adlard, P. A., Finkelstein, D. I. & Bush, A. I. (2015). Clioquinol rescues Parkinsonism and dementia phenotypes of the tau knockout mouse. Neurobiology of Disease, 81, pp.168-175. https://doi.org/10.1016/j.nbd.2015.03.015.

Clioquinol rescues parkinsonism and dementia phenotypes of the tau knockout mouse

Peng Lei*, Scott Ayton, Ambili Thoppuvalappil Appukuttan, Irene Volitakis, Paul A. Adlard, David I. Finkelstein, Ashley I. Bush*

Oxidation Biology Unit, Florey Institute of Neuroscience and Mental Health, The University of Melbourne, Victoria, Australia

*Correspondence to

Dr. Peng Lei
Address: Kenneth Myer Building, 30 Royal Pde, The University of Melbourne, Parkville, Victoria 3010, AUSTRALIA
Phone: +61 (0)3 9035 6686
E-mail: peng.lei@florey.edu.au

Or

Prof Ashley I. Bush
Address: Kenneth Myer Building, 30 Royal Pde, The University of Melbourne, Parkville, Victoria 3010, AUSTRALIA
Phone: +61 (0)3 9035 6532
E-mail: ashley.bush@florey.edu.au

Highlights

- Clioquinol rescues parkinsonism phenotype and increases nigral tyrosine hydroxylase activity in aged tau knockout mouse
- Clioquinol rescues cognitive phenotype in aged tau knockout mouse and elevates neurotrophins
- Clioquinol selectively reverses iron accumulation in aged tau knockout mouse

Abstract

Iron accumulation and tau protein deposition are pathological features of Alzheimer's (AD) and Parkinson's diseases (PD). Soluble tau protein is lower in affected regions of these diseases, and we previously reported that tau knockout mice display motor and cognitive behavioral abnormities, brain atrophy, neuronal death in substantia nigra, and iron accumulation in the brain that all emerged between 6 and 12 months of age. This argues for a loss of tau function in AD and PD. We also showed that treatment with the moderate iron chelator, clioquinol (CQ) restored iron levels and prevented neuronal atrophy and attendant behavioral decline in 12 month old tau KO mice when commenced prior to the onset of deterioration (6 months). However, therapies for AD and PD will need to treat the disease once it is already manifest. So, in the current study, we tested whether CQ could also rescue the phenotype of mice with a developed phenotype. We found that 5 months treatment of symptomatic (13 month old) tau KO mice with CQ increased nigral tyrosine hydroxylase phosphorylation (which induces activity) and reversed the motor deficits. Treatment also reversed cognitive deficits and raised BDNF levels in hippocampus, which was accompanied by attenuated brain atrophy, and reduced iron content in the brain. These data raise the possibility that lowering brain iron levels in symptomatic patients could reverse neuronal atrophy and improve brain function, possibly by elevating neurotrophins.

Key words: Tau, Parkinson's disease, Alzheimer's disease, clioquinol, Iron

Introduction

Alzheimer's disease (AD) and Parkinson's disease (PD) are both age-dependent chronic neurological disorders, which pathologically feature protein aggregation and iron accumulation in the affected brain regions (1, 2). Despite significant efforts made in last two decades, there is still no disease modifying treatment for either disease. Most recently, a number of large Phase III clinical trials targeting β-amyloid aggregation, a key feature of AD, were conducted, but failed to demonstrate efficiency (3-5). It is therefore of crucial importance to search for alternative drug targets that may modify the disease symptoms.

Tau protein is extensively implicated in the pathogenesis of AD and considered as a potential drug target (6). Recent genome-wide association studies identified a significant association between the MAPT locus and sporadic PD (7, 8), indicating a possible pathological link between tau and PD. The link was supported by pathological findings including the interaction between α-synuclein and tau, and the presence of tau in the Lewy bodies of typical PD (7, 9). Furthermore, tau mutations cause atypical PD syndromes, such as progressive supranuclear palsy, and corticobasal degeneration (6). While the hyperphosphorylation of tau causes toxicity (10), increasing evidence also supports a possible role for functional loss of tau protein in both diseases, as soluble tau is reduced in the affected regions in both disorders (11-13). We previously reported that tau knockout mouse display progressive motor and cognitive behavioral abnormities, brain weight loss and brain-wide atrophy, loss of key proteins involved in memory formation, neuronal death in substantia nigra (SN), dopamine loss and tyrosine hydroxylase (TH) terminal loss in the caudate-putamen (CPu), as well as iron accumulation in the brain; all of which are features of neurodegeneration (11, 14). Others showed that tau knockout mice (on a different genetic background) display progressive motor and cognitive deficits, in association with loss of microtubule associated proteins other than tau, and the phenotypes can be prevented by an anti-oxidant (15). Although the cognitive phenotypes of tau knockout mouse may depend on its genetic background and food (16, 17), the tau knockout mouse remains to be a useful model of aged-associated neurodegeneration which can be utilized for drug discovery.

We have previously shown that 5-chloro-7-iodo-quinolin-8-ol (clioquinol, CQ) treatment prevented the progression of these phenotypes (treatment from 6-months of age), through prevention of iron accumulation in key regions of the brain (11). CQ is an 8-hydroxyquinoline derivative that was widely used as an anti-parasitic agent until the 1970s, when it was withdrawn because of suspected severe adverse effects in a Japanese population (18, 19). It was rediscovered in 2000s to be a drug candidate for Alzheimer's disease since treatment with CQ rapidly reduced plaques in Tg2576 transgenic mice (20). It was later found that CQ also showed beneficial effects in cellular and animal models of PD (11, 21-23), Huntington's disease (HD) (24), cancer (25-27), and it can protect against aging sequelae (28, 29). It also was tested in a phase 2 clinical trial in AD, which reported that it was well tolerated and that treatment slowed cognitive deterioration (30). It is proposed that CQ is neuroprotective, and functions by chaperoning the biometals (31, 32), involved in disease pathogenesis (33). More specifically, CQ is found to be a copper and zinc ionophore (32), and a moderate iron chelator (21). The second generation of CQ, PBT2, was reported to be safe and beneficial for AD and HD patients in Phase II clinical trials (34, 35). Other iron chelation therapies have also been tested preclinically and clinically for AD and PD, and showed positive outcomes (21, 36-45).

Our previous results demonstrating the efficacy of CQ in tau KO mice were from a prevention experimental paradigm, where the drug administration commenced before symptom onset. But a therapy for neurodegenerative disorders will require drug treatment after disease manifestation. So, in the current study, we explored whether CQ treatment to symptomatic (13 month old) tau knockout mice would rescue behavioral, biochemical and neuroanatomical deficits.

Results

CQ rescues behavioral disability of symptomatic tau KO mice

Tau knockout mice commenced CQ therapy (30mg/kg/day) at 13-months of age and were treated for 5 months. Mice were monitored every three weeks by accelerating rotarod test as well as pole

test during the CQ treatment period. The mice were symptomatic at the commencement of the study, displaying impairment in rotarod, pole test and Y-maze, but had normal body weight, when compared to 12-month old wild-type historic controls (11, 14).

CQ treatment did not alter the body weight of mice compared to sham-treatment over the treatment period (**Fig 1a**), but treatment significantly improved motor performance at each interval on rotarod (**Fig 1b**) and pole test (**Fig 1c**). In the rotarod test, CQ-treated mice could maintain balance on the rod significantly longer after 6 weeks treatment compared to sham-treated mice (p=0.044), or the starting point (p=0.009 for 21 days; p<0.001 for 42 days, 63 days, or 84 days; **Fig 1b**). The improvement was maintained over the remainder of the treatment interval (p=0.006 at 63 days; p=0.041 at 84 days). CQ treatment also improved pole test performance after 3 weeks; treated mice required significantly shortened time to turn on the pole (p=0.009 compared to sham-treated; p<0.001 compared to starting point; **Fig 1c**). Repeated pole tests did not cause changes in performance for sham-treated mice, consistent with previous findings (46).

4 months of CQ-treatment also caused an improvement in the frequency of entries into the novel arm of the Y-maze compared to sham-treated mice (p=0.047, **Fig 1d**), without affecting the total entry time in Y maze test (data not shown), indicating that CQ treatment improved cognitive function.

Motor and cognitive improvement by CQ is associated with restored iron levels in associated brain regions

We previously showed that CQ reduced iron levels in the primary neuronal culture, and prevented iron accumulation in the brain of tau knockout mouse (11). In the current study, tau knockout mice, which have elevated brain iron at 13 months when the treatment commenced (11), showed significantly less iron content in hippocampus (-20%, p=0.0047) and SN (-17%, p=0.0102) after 5 months of treatment (at 18-months of age, **Fig 2a**) compared to sham-treated mice. Iron levels in liver were unaffected (**Fig 2a**). Copper and zinc levels in all examined brain regions were

unaltered by CQ treatment (**Fig 2b-c**), consistent with previous findings (11).

Increased TH activity is associated with improvement of motor function by CQ

Previously we found that CQ prevented functional motor decline by preventing iron accumulation, which then preserved the SN neurons (11). Iron chelation was previously reported to reverse the motor disability by restoring SN neuron number, striatal dopamine levels and TH connection in a mouse model of PD (47, 48). We found that the improvement in motor and cognitive phenotype that we observed when CQ treatment was initiated after symptom onset was not associated with a restoration in SN neuron number (**Fig 3a**), or striatal dopamine levels (**Fig 3b**), although the treatment did normalize iron elevation in the nigra and hippocampal brain regions (**Fig 2a**). Lowering iron increases TH phosphorylation and enzyme activity (49, 50). Indeed, we found that CQ treatment increased the phosphorylation of TH at Ser40 (+101%, p=0.016), without affecting TH total protein expression in SN (**Fig 3c-e**). In addition, we found that the striatal region of CQ-treated mice was significantly larger than sham-treated mice (+13%, p=0.047), and TH expression in the striatum was significantly increased comparing to sham-treated mice (+36%, p=0.037; **Fig 3f-h**). Although steady-state dopamine levels were not increased in the striatum of the CQ-treated mice, the increase in phosphorylated TH in the nigra, together with increased TH density on the striatal projection field, indicates that the improved motor performance in the CQ-treated animals may be due to increase in dopamine delivery efficiency.

CQ therapy attenuates brain atrophy and increases neurotrophins

We previously found that tau knockout mice at 12 months of age had significantly lighter brains compared to WT, reflecting brain atrophy (11). In the current study, treatment with CQ did not alter brain wet weight (**Fig 4a**). However, consistent with improved cognitive performance in the Y-maze, CQ treatment of tau knockout mice from 13 to 18 months of age rescued the enlargement of lateral ventricle (-43%, p=0.032), cortical thickness (+6.5%, p=0.043; **Fig 4b**), in addition to preventing loss of CPu (**Fig. 3g**). Corpus callosum thickness (**Fig 4b**), the thickness of

the cerebellar granular layer, and 4th ventricular area (data not shown) were unaltered.

We previously found that key proteins involved in memory formation were reduced in 12-month old tau knockout mice (11). Here, we found that treatment with CQ restored the levels of BDNF (+33.5%, p=0.011) and proBDNF (+31.4%, p=0.046; **Fig 4c-e**) in the hippocampus, consistent with improved cognitive performance and attenuated brain atrophy.

Discussion

Our current study reconfirms the cognitive and motor neurodegenerative phenotype of tau knockout mice at a more advanced age than our previous reports (11, 14). Since we previously demonstrated the phenotype in two separate cohorts (11, 14), here we included only historic controls as dimensional comparators for the phenotype, which is a caveat in estimating the degree of pathology associated with the mutant. Nevertheless, the surprising finding was that despite the presence of established neurodegenerative features of atrophy and nigral dopaminergic loss, CQ treatment could reverse some of these losses. This indicates that some trophic mechanism has likely been induced.

We found that CQ treatment increased BDNF levels in hippocampus (**Fig 4c-e**), and increased TH activity in SN (**Fig 3c-e**) of mice that already expressed AD and PD phenotypes. A loss-of-function mutation of BDNF impairs cognitive function (51). We hypothesize that CQ induces increased BDNF by lowering iron levels (**Fig. 2a**), because previously iron chelators have been reported to improve cognitive function and simultaneously increase brain BDNF in the treatment of various neurodegenerative animal models (52-54). Further mechanistic studies of the relationship between BDNF expression or processing and cellular iron levels are warranted. Although CQ has been previously shown to affect copper and zinc, we excluded this as neither copper nor zinc were affected by loss-of-tau (11), or CQ treatment in this study (**Fig 2**). Correcting iron overload lowers the oxidative stress burden of neurons by preventing hydroxyl radical formation by labile iron (1). Reducing oxidative stress can therefore attenuate the

progression of neuronal loss, and, indeed, antioxidant treatment in tau knockout mice has been reported to rescue the phenotype (15).

TH phosphorylation (and activity) is known to be regulated by iron (49), and increased TH activity enhances dopaminergic function (55, 56). We hypothesize that iron chelation by CQ in areas where cell loss is already manifest promotes neurotrophic sequelae to combat neurodegeneration. It is conceivable, therefore, that reducing iron overload in AD and PD might arrest future decline by preventing oxidative stress, maximizing synaptic dopamine turnover, increasing neurotrophins, and lead to improved motor and cognitive behaviors.

No disease modifying therapy currently exists for AD or PD. As no prognostic biomarker with sufficient accuracy can determine who will develop the disease, a disease modifying therapy for these disorders must be effective after symptomatic onset, where neuronal loss has begun. Iron could be a common target for these diseases. In AD, we found that reduced tau prevented APP trafficking to cell surface where it is needed to facilitate iron export by ferroportin (11, 57-59). In PD, we found evidence that nitric oxide suppressed APP expression, and, with loss of soluble tau further limiting the presentation of APP in cell surface, results in nigral iron accumulation (11, 60). Here we show using the tau knockout mouse model that normalizing iron content in the brain has the potential to confer disease-modifying benefit after symptom onset. CQ was tested in a pilot randomized phase 2 clinical trial of AD, and reported significant attenuation of cognitive deterioration over 9 months (30). Other iron chelators, deferiprone and desferioxamine have shown positive results in phase II clinical trials of PD and AD respectively (36, 45) - some of the few examples of positive clinical trial data for these diseases. The current study supports iron mitigation as a potential strategy to treat AD and PD that warrants further investigation.

Methods

Mice and mice tissue preparation. All mice were housed in a conventional animal facility according to standard animal care protocols and fed standard laboratory chow (Meat Free Rat and

Mouse Diet, Specialty Feeds, Australia) and tap water *ad libitum*. All animal procedures were approved by the Florey Institute animal ethics committee (10-017) and were performed in accordance with the National Health and Medical Research Council guidelines. Tau knockout mice (Dawson et al. 2001) and background C57Bl6/SV129 mice were raised under the same conditions, maintained homozygously, and mutants were backcrossed to the parental inbred strain every 3 generations. To obtain the mouse brain, mice were euthanized with an overdose of sodium pentobarbitone (Lethabarb, 100mg/kg) and perfused with ice-cold saline. Body weight and total brain wet weight were recorded. The right brain hemisphere was micro-dissected and stored at -80°C until required. The left brain hemisphere was fixed in 4% paraformaldehyde for 24 h, and then transferred to 30% Sucrose + PBS (pH 7.4) and kept at 4°C overnight for tyrosine hydroxylase (TH) immunohistochemistry and brain section analysis.

CQ treatment. Tau knockout mice commenced CQ feeding from 13-months of age. Mice were fed a diet of rodent chow mixed with 0.25g/kg (equivalent to dosing ≈30mg/kg/day) of CQ (Specialty Feeds, Western Australia) for 5 months and then sacrificed. Performance tests were performed every 3-4 weeks to monitor the effects of CQ.

Anatomical morphology from brain slice. The anatomical morphology was examined as previously described (11). Briefly, CPu and cerebellum sections from mice were sectioned using a Leica Cryostat set at 50μm thickness and areas of interest were measured using Image-J (v1.49b, NIH), using landmarks (anterior commissure for CPu and flocculus for cerebellum) to identify the level of coronal sectioning (bregma 0.26±0.01mm and bregma -6.12±0.01mm). Two sections per mouse per area were analyzed. CPu area was defined by the boundaries of corpus callosum, lateral ventricle, and anterior commissure. Corpus callosum, neocortical and cerebellar cortical thicknesses were averaged from 5 measurements. All quantifications were blinded.

Y maze test. Y maze test was performed as previously described (11). Briefly, all mice were subjected to a 2-trial Y-maze test separated by a 1-h inter-trial interval to assess spatial recognition memory, with all testing performed during the light phase of the circadian cycle.

Behaviors were recorded on video during a 5 min trial and Ethovision video-tracking system (Noldus, Netherlands) was used for analysis. Data are expressed as the percentage of frequency for novel arm entries made during the 5-min trial.

Pole Test. Pole test was performed as previously described (11). Briefly, mice were placed vertically on a 30cm vertical, 1cm diameter pole, where mice make an 180^{o} turn and return to the base of the pole, which is placed in their home cage. On the day prior to testing (day 1), the animals were habituated to the pole and were allowed five consecutive trials. Animals were then recorded via digital video on the test day (day 2). The amount of time was recorded for the interval for the mouse to turn toward the ground (time to turn), and for the interval to reach the ground (time to finish). Each mouse underwent five trials and the average was used in analysis. When mice were unable to turn and fall down from the pole, it is determined as incomplete trial.

Accelerated rotarod test. Rotarod test was performed as previously described (11). Briefly, mice were assessed using a Panlab Rotarod apparatus in an accelerating model with triplicate measurements (maximum time of 2.5 min; speed increases every 8s). The time on the rod as well as the final speed of the rod was recorded and the triplicates averaged for analysis.

Tyrosine hydroxylase immunohistochemistry. TH immunohistochemistry was performed as previously described (11). Briefly, brains were immersion fixed (4% paraformaldehyde) overnight and then cryoprotected in 30% sucrose/PBS until frozen sectioned on a calibrated Leica Cryostat in 30 μm sections for SN. Sections (1:3 series) were collected through the SN pars compacta (SNpc) (anteroposterior -2.92 to -3.64 mm from bregma, Mouse Atlas Figure 55 to Figure 61), generating 8 sections per mouse (the second of the three sections was analyzed). After brief fixation (4% paraformaldehyde for 30 seconds), the sections were blocked in 3% normal goat serum (Millipore) and incubated with primary anti-TH rabbit polyclonal (1:3000, Millipore) overnight. The sections were then incubated with goat anti-rabbit secondary HRP-conjugated antibody for 3 hours (Millipore), followed by diaminobenzidine solution (1% w/v in PBS + 1% w/v $CoCl_2$, 1% w/v $NiSO_4$) + 3% w/v hydrogen peroxide (1:3000). SN TH immunostained slides

were counter-stained with Neutral Red to visualize the Nissl substance in all neurons, and then were mounted on Superfrost-Plus slides. The intensity of TH in the CPu was then quantified by ImageJ (1.49b, NIH), using cortex as background control.

Stereological estimation of nigra neurons. SN neuron number was estimated as previously described (11). Briefly, TH-positive and TH-negative, Nissl-positive neurons were scored according to the optical fractionator rules, using an unbiased counting frame of x=35 μm, y = 45 μm at regular intervals on a sampling grid of x=140 μm, y=140 μm, viewed with a 60 x 1.3 N.A. oil objective (DMLB Leica Microscope) by the morphometry and design-based stereology software package (Stereo Investigator 10.04, Microbrightfield, Colchester, VT). The coefficients of error (CE) and coefficients of variance (CV) were calculated as estimates of precision and values of <0.1 were accepted.

Dopamine and Dopac measurement. Dopamine metabolites were measured as previously described (11). Briefly, CPu tissues were homogenized in HPLC sample buffer (0.4M perchloric acid, 0.15% sodium metabisulfite and 0.05% EDTA) before centrifugation at 10,000 g at 4 ˚C for 10 minutes. Supernatants were used for dopamine measurement by a HPLC system (ESA Biosciences; model 584) coupled to an electrochemical detector (ESA Biosciences; Coulochem III detector) (E1:-150 mV, E2:+220 mV, and guard cell: +250 mV). 50 μL was injected onto a MD-150 reverse phase C18 column (ESA Biosciences) and elution was performed at a flow rate of 0.6 ml/min in the mobile phase (75 mM sodium dihydrogen phosphate, 1.7 mM 1-octanesulfonic acid sodium salt, 100 mL/L triethylamine, 25 mM EDTA, 10% acetonitrile, pH 3). Peaks were identified by retention times set to known standards. Data were normalized to wet weight tissue.

Western Blot. Samples from each experiments were homogenized in PBS (pH=7.4) with EDTA-free protease inhibitor cocktail (1:50, Roche) + phosphatase inhibitors I and II (1:1000) and centrifuged at 40,000 g for 30 minutes. Protein concentration was determined by BCA protein assay (Pierce). Aliquots of homogenate with equal protein concentrations were separated

in 4-12% bis-Tris gels with NuPAGE MES running buffer (Invitrogen), and transferred to nitrocellulose membranes by iBlot (Invitrogen). The membranes were blocked with milk (10% w/v) and probed with appropriate primary and secondary IgG-HRP conjugated antibodies (Dako). Enhanced chemiluminescence detection system (GE Healthcare) was used for developing and Fujifilm LAS-3000 was used for visualization. Densitometry quantification of immunoreactive signals was performed by ImageJ (1.49b, NIH) and normalized to the relative amount of β-actin and expressed as percentage of the mean of the control group. The following antibodies were used in current study: anti-β-actin (Sigma); anti-BDNF (Abcam); anti-ProBDNF (Biosensis); anti-TH (Millipore); anti-pTH-Ser40 (PhosphoSolutions).

Metal Analysis. Metal content was measured as previously described (11). Briefly, samples from each experimental condition were freeze-dried, and then re-suspended in 69% nitric acid (ultraclean grade, Aristar) overnight. The samples were then heated for 20 min at 90 ˚C, and equivalent volume of hydrogen peroxide (30%, Merck) was added for further 15 min incubation at 70 ˚C. The samples were diluted in double-distilled water and assayed by inductively coupled plasma mass spectrometer (Ultramass 700, Varian). Each sample was measured in triplicate and the concentrations determined from the standard curve were normalized to wet tissue weight.

Statistics. Statistical analysis was carried out in Prism 6 (GraphPad Software Inc). All tests were two-tailed, with the level of significance set at 0.05. Detailed tests used in each experiment are described in Figure legends.

Competing Interests

Drs Adlard and Finkelstein are shareholders in and paid scientific consultants for Prana Biotechnology Pty Ltd. Dr. Bush is a shareholder in Prana Biotechnology Pty Ltd., Eucalyptus Pty Ltd., Mesoblast Pty Ltd., Brighton Biotech Inc and a paid consultant for Collaborative Medicinal Developments LLC and Brighton Biotech Inc.

Authors' Contributions

Scientific concept: PL, AIB. Experimental design: PL, PAA, DIF, AIB. Experiments: PL, SA, ATA, IV, PAA. Manuscript preparation: PL, SA, AIB. Manuscript edit: all authors.

Acknowledgments

Supported by funds from the Australian Research Council, the National Health & Medical Research Council (NHMRC) of Australia, the Cooperative Research Center for Mental Health, Alzheimer's Australia Dementia Research Foundation, and Melbourne Early Career Researcher Grants Scheme. Florey Institute of Neuroscience and Mental Health acknowledges the strong support from the Victorian Government and in particular the funding from the Operational Infrastructure Support Grant.

References

1. Hare D, Ayton S, Bush A, Lei P. A delicate balance: Iron metabolism and diseases of the brain. Front Aging Neurosci. 2013;5:34.
2. Ayton S, Lei P, Bush AI. Biometals and Their Therapeutic Implications in Alzheimer's Disease. Neurotherapeutics. 2014.
3. Doody RS, Raman R, Farlow M, Iwatsubo T, Vellas B, Joffe S, et al. A phase 3 trial of semagacestat for treatment of Alzheimer's disease. N Engl J Med. 2013;369(4):341-50.
4. Doody RS, Thomas RG, Farlow M, Iwatsubo T, Vellas B, Joffe S, et al. Phase 3 trials of solanezumab for mild-to-moderate Alzheimer's disease. N Engl J Med. 2014;370(4):311-21.
5. Salloway S, Sperling R, Fox NC, Blennow K, Klunk W, Raskind M, et al. Two phase 3 trials of bapineuzumab in mild-to-moderate Alzheimer's disease. N Engl J Med. 2014;370(4):322-33.
6. Gozes I. Tau pathology and future therapeutics. Curr Alzheimer Res. 2010;7(8):685-96.
7. Lei P, Ayton S, Finkelstein DI, Adlard PA, Masters CL, Bush AI. Tau protein: relevance to Parkinson's disease. The international journal of biochemistry & cell biology. 2010;42(11):1775-8.
8. Nalls MA, Pankratz N, Lill CM, Do CB, Hernandez DG, Saad M, et al. Large-scale meta-analysis of genome-wide

association data identifies six new risk loci for Parkinson's disease. Nature genetics. 2014;46(9):989-93.
9. Arima K, Hirai S, Sunohara N, Aoto K, Izumiyama Y, Uéda K, et al. Cellular co-localization of phosphorylated tau- and NACP/alpha-synuclein-epitopes in lewy bodies in sporadic Parkinson's disease and in dementia with Lewy bodies. Brain Res. 1999;843(1-2):53-61.
10. Morris M, Maeda S, Vossel KA, Mucke L. The many faces of tau. Neuron. 2011;70(3):410-26.
11. Lei P, Ayton S, Finkelstein DI, Spoerri L, Ciccotosto GD, Wright DK, et al. Tau deficiency induces parkinsonism with dementia by impairing APP-mediated iron export. Nat Med. 2012;18(2):291-5.
12. Kosik KS, Crandall JE, Mufson EJ, Neve RL. Tau in situ hybridization in normal and Alzheimer brain: localization in the somatodendritic compartment. Annals of neurology. 1989;26(3):352-61.
13. Zhukareva V, Vogelsberg-Ragaglia V, Van Deerlin VM, Bruce J, Shuck T, Grossman M, et al. Loss of brain tau defines novel sporadic and familial tauopathies with frontotemporal dementia. Ann Neurol. 2001;49(2):165-75.
14. Lei P, Ayton S, Moon S, Zhang Q, Volitakis I, Finkelstein DI, et al. Motor and cognitive deficits in aged tau knockout mice in two background strains. Mol Neurodegener. 2014;9(1):29.
15. Ma QL, Zuo X, Yang F, Ubeda OJ, Gant DJ, Alaverdyan M, et al. Loss of MAP function leads to hippocampal synapse loss and deficits in the Morris Water Maze with aging. J Neurosci. 2014;34(21):7124-36.
16. Gheyara AL, Ponnusamy R, Djukic B, Craft RJ, Ho K, Guo W, et al. Tau reduction prevents disease in a mouse model of Dravet syndrome. Annals of neurology. 2014;76(3):443-56.
17. Morris M, Hamto P, Adame A, Devidze N, Masliah E, Mucke L. Age-appropriate cognition and subtle dopamine-independent motor deficits in aged Tau knockout mice. Neurobiol Aging. 2013;34(6):1523-9.
18. Asao M. Clioquinol and S.M.O.N.: Reanalysis of original data. Lancet. 1979;1(8113):446.
19. Nakae K, Yamamoto S, Igata A. Subacute myelo-optico-neuropathy (S.M.O.N.) in Japan. A community survey. Lancet. 1971;2(7723):510-2.
20. Cherny RA, Atwood CS, Xilinas ME, Gray DN, Jones WD, McLean CA, et al. Treatment with a copper-zinc chelator markedly and rapidly inhibits beta-amyloid accumulation in Alzheimer's disease transgenic mice. Neuron. 2001;30(3):665-76.
21. Kaur D, Yantiri F, Rajagopalan S, Kumar J, Mo JQ, Boonplueang R, et al. Genetic or pharmacological iron chelation prevents MPTP-induced neurotoxicity in vivo: a novel therapy for Parkinson's disease. Neuron. 2003;37(6):899-909.
22. Kaur D, Rajagopalan S, Andersen JK. Chronic expression of H-ferritin in dopaminergic midbrain neurons results in an age-related expansion of the labile iron pool and subsequent neurodegeneration: implications for Parkinson's disease. Brain Res. 2009;1297:17-22.
23. Tardiff DF, Tucci ML, Caldwell KA, Caldwell GA, Lindquist S. Different 8-hydroxyquinolines protect models of TDP-43 protein, alpha-synuclein, and polyglutamine proteotoxicity through distinct mechanisms. J Biol Chem. 2012;287(6):4107-20.
24. Nguyen T, Hamby A, Massa SM. Clioquinol down-regulates mutant huntingtin expression in vitro and mitigates pathology in a Huntington's disease mouse model. Proc Natl Acad Sci U S A. 2005;102(33):11840-5.
25. Chen D, Cui QC, Yang H, Barrea RA, Sarkar FH, Sheng S, et al. Clioquinol, a therapeutic agent for Alzheimer's disease, has proteasome-inhibitory, androgen receptor-suppressing, apoptosis-inducing, and antitumor activities in human prostate cancer cells and xenografts. Cancer Res. 2007;67(4):1636-44.
26. Ding WQ, Yu HJ, Lind SE. Zinc-binding compounds induce cancer cell death via distinct modes of action. Cancer Lett. 2008;271(2):251-9.

27. Yu H, Zhou Y, Lind SE, Ding WQ. Clioquinol targets zinc to lysosomes in human cancer cells. Biochem J. 2009;417(1):133-9.
28. Wang Y, Branicky R, Stepanyan Z, Carroll M, Guimond M-P, Hihi A, et al. The anti-neurodegeneration drug clioquinol inhibits the aging-associated protein CLK-1. J Biol Chem. 2009;284(1):314-23.
29. Adlard PA, Sedjahtera A, Gunawan L, Bray L, Hare D, Lear J, et al. A novel approach to rapidly prevent age-related cognitive decline. Aging Cell. 2014;13(2):351-9.
30. Ritchie CW, Bush AI, Mackinnon A, Macfarlane S, Mastwyk M, MacGregor L, et al. Metal-protein attenuation with iodochlorhydroxyquin (clioquinol) targeting Abeta amyloid deposition and toxicity in Alzheimer disease: a pilot phase 2 clinical trial. Archives of neurology. 2003;60(12):1685-91.
31. Li C, Wang J, Zhou B. The metal chelating and chaperoning effects of clioquinol: insights from yeast studies. J Alzheimers Dis. 2010;21(4):1249-62.
32. Adlard PA, Cherny RA, Finkelstein DI, Gautier E, Robb E, Cortes M, et al. Rapid restoration of cognition in Alzheimer's transgenic mice with 8-hydroxy quinoline analogs is associated with decreased interstitial Abeta. Neuron. 2008;59(1):43-55.
33. Ayton S, Lei P, Bush AI. Metallostasis in Alzheimer's disease. Free Radic Biol Med. 2013;62:76-89.
34. Lannfelt L, Blennow K, Zetterberg H, Batsman S, Ames D, Harrison J, et al. Safety, efficacy, and biomarker findings of PBT2 in targeting Abeta as a modifying therapy for Alzheimer's disease: a phase IIa, double-blind, randomised, placebo-controlled trial. Lancet neurology. 2008;7(9):779-86.
35. Faux NG, Ritchie CW, Gunn AP, Rembach A, Tsatsanis A, Bedo J, et al. PBT2 rapidly improves cognition in Alzheimer's Disease: additional phase II analyses. J Alzheimers Dis. 2010;20(2):509-16.
36. Devos D, Moreau C, Devedjian JC, Kluza J, Petrault M, Laloux C, et al. Targeting chelatable iron as a therapeutic modality in Parkinson's disease. Antioxidants & redox signaling. 2014;21(2):195-210.
37. Ben-Shachar D, Eshel G, Finberg JP, Youdim MB. The iron chelator desferrioxamine (Desferal) retards 6-hydroxydopamine-induced degeneration of nigrostriatal dopamine neurons. J Neurochem. 1991;56(4):1441-4.
38. Zheng H, Gal S, Weiner LM, Bar-Am O, Warshawsky A, Fridkin M, et al. Novel multifunctional neuroprotective iron chelator-monoamine oxidase inhibitor drugs for neurodegenerative diseases: in vitro studies on antioxidant activity, prevention of lipid peroxide formation and monoamine oxidase inhibition. J Neurochem. 2005;95(1):68-78.
39. Zheng H, Weiner LM, Bar-Am O, Epsztejn S, Cabantchik ZI, Warshawsky A, et al. Design, synthesis, and evaluation of novel bifunctional iron-chelators as potential agents for neuroprotection in Alzheimer's, Parkinson's, and other neurodegenerative diseases. Bioorg Med Chem. 2005;13(3):773-83.
40. Kupershmidt L, Amit T, Bar-Am O, Youdim MB, Weinreb O. The novel multi-target iron chelating-radical scavenging compound M30 possesses beneficial effects on major hallmarks of Alzheimer's disease. Antioxidants & redox signaling. 2012;17(6):860-77.
41. Ayton S, Lei P, Duce JA, Wong BX, Sedjahtera A, Adlard PA, et al. Ceruloplasmin dysfunction and therapeutic potential for Parkinson disease. Annals of neurology. 2013;73(4):554-9.
42. Guo C, Wang P, Zhong ML, Wang T, Huang XS, Li JY, et al. Deferoxamine inhibits iron induced hippocampal tau phosphorylation in the Alzheimer transgenic mouse brain. Neurochem Int. 2013;62(2):165-72.
43. Zhu W, Li X, Xie W, Luo F, Kaur D, Andersen JK, et al. Genetic iron chelation protects against proteasome inhibition-induced dopamine neuron degeneration. Neurobiology of disease. 2010;37(2):307-13.
44. Guo C, Wang T, Zheng W, Shan ZY, Teng WP, Wang ZY. Intranasal deferoxamine reverses iron-induced memory deficits and inhibits amyloidogenic APP processing in a transgenic mouse model of Alzheimer's disease. Neurobiol

Aging. 2013;34(2):562-75.
45. Crapper McLachlan DR, Dalton AJ, Kruck TP, Bell MY, Smith WL, Kalow W, et al. Intramuscular desferrioxamine in patients with Alzheimer's disease. Lancet. 1991;337(8753):1304-8.
46. Paylor R, Spencer CM, Yuva-Paylor LA, Pieke-Dahl S. The use of behavioral test batteries, II: effect of test interval. Physiol Behav. 2006;87(1):95-102.
47. Zhu W, Xie W, Pan T, Xu P, Fridkin M, Zheng H, et al. Prevention and restoration of lactacystin-induced nigrostriatal dopamine neuron degeneration by novel brain-permeable iron chelators. FASEB J. 2007;21(14):3835-44.
48. Gal S, Zheng H, Fridkin M, Youdim MB. Restoration of nigrostriatal dopamine neurons in post-MPTP treatment by the novel multifunctional brain-permeable iron chelator-monoamine oxidase inhibitor drug, M30. Neurotoxicity research. 2010;17(1):15-27.
49. Beard JL, Killick T, Gonzales E, Bianco L. Reductions in the Labile Iron Pool activate PKC and alter monoamine metabolism. FASEB J. 2006;20(4):A193-A.
50. Dunkley PR, Bobrovskaya L, Graham ME, von Nagy-Felsobuki EI, Dickson PW. Tyrosine hydroxylase phosphorylation: regulation and consequences. J Neurochem. 2004;91(5):1025-43.
51. Egan MF, Kojima M, Callicott JH, Goldberg TE, Kolachana BS, Bertolino A, et al. The BDNF val66met polymorphism affects activity-dependent secretion of BDNF and human memory and hippocampal function. Cell. 2003;112(2):257-69.
52. Adlard PA, Parncutt J, Lal V, James S, Hare D, Doble P, et al. Metal chaperones prevent zinc-mediated cognitive decline. Neurobiology of disease. 2014.
53. Bar-Am O, Amit T, Kupershmidt L, Aluf Y, Mechlovich D, Kabha H, et al. Neuroprotective and neurorestorative activities of a novel iron chelator-brain selective monoamine oxidase-A/monoamine oxidase-B inhibitor in animal models of Parkinson's disease and aging. Neurobiol Aging. 2014.
54. Kupershmidt L, Weinreb O, Amit T, Mandel S, Bar-Am O, Youdim MB. Novel molecular targets of the neuroprotective/neurorescue multimodal iron chelating drug M30 in the mouse brain. Neuroscience. 2011;189:345-58.
55. Salvatore MF, Zhang JL, Large DM, Wilson PE, Gash CR, Thomas TC, et al. Striatal GDNF administration increases tyrosine hydroxylase phosphorylation in the rat striatum and substantia nigra. J Neurochem. 2004;90(1):245-54.
56. Yabuki Y, Ohizumi Y, Yokosuka A, Mimaki Y, Fukunaga K. Nobiletin treatment improves motor and cognitive deficits seen in MPTP-induced Parkinson model mice. Neuroscience. 2014;259:126-41.
57. Duce JA, Tsatsanis A, Cater MA, James SA, Robb E, Wikhe K, et al. Iron-export ferroxidase activity of β-amyloid precursor protein is inhibited by zinc in Alzheimer's disease. Cell. 2010;142(6):857-67.
58. Wong BX, Tsatsanis A, Lim LQ, Adlard PA, Bush AI, Duce JA. beta-Amyloid precursor protein does not possess ferroxidase activity but does stabilize the cell surface ferrous iron exporter ferroportin. PLoS ONE. 2014;9(12):e114174.
59. Wong BX, Ayton S, Lam LQ, Lei P, Adlard PA, Bush AI, et al. A comparison of ceruloplasmin to biological polyanions in promoting the oxidation of Fe under physiologically relevant conditions. Biochim Biophys Acta. 2014;1840(12):3299-310.
60. Ayton S, Lei P, al. E. Parkinson's Disease Iron Deposition Caused by Nitric Oxide-Induced Loss of beta-Amyloid Precursor Protein. J Neurosci. 2015.

Figure legends

Figure 1. CQ treatment from 13 months of age rescues behavioral impairment in tau knockout mice. **a**) No differences were found in the body weights of mice treated with CQ. Two-way ANOVA: no significant effects of duration ($p = 0.929$), treatment ($p = 0.934$), nor interaction ($p = 0.791$). **b**) Rotarod test showed that CQ treatment rescued motor performance. Two-way ANOVA: treatment duration ($p < 0.001$), treatment ($p = 0.012$) effects and interaction ($p = 0.036$). **c**) CQ rescued pole test performance. Two-way ANOVA: treatment duration ($p < 0.001$), treatment ($p < 0.001$) effects and interaction ($p = 0.033$). **d**) Cognitive impairment in tau knockout mice was rescued by CQ treatment, evidenced by the significant elevation of frequency to enter the novel arm in Y maze test (two-tailed t-test). Dotted lines indicate our previously-reported mean values for wild-type mice at 12 months of age as a comparator (11). n=7 per treatment. Data are means ± S.E.M. *p<0.05, **p<0.01, versus the performance of sham-treated mice (Sidak post hoc test). ##p< 0.01, ###p< 0.001, versus the starting point (Sidak post hoc test).

Figure 2. Metal content in sham-treated and CQ-treated tau knockout mice. **a-c**) Metal levels in hippocampus, SN and liver of tau KO mice after treatment with CQ for 5 months from 12.5-month-old. Significant reductions of iron (**a**) in the brain were found after CQ-treatment (p=0.003 for hippocampus, and p=0.007 for SN, two-tailed t-test). No differences of copper (**b**) or zinc (**c**) were found in CQ-treated mice compared to sham-treated mice. Dotted lines indicate our previously-reported mean values for wild-type mice at 12 months of age as a comparator (11). n=7 per group. Data are means ± S.E.M. **p<0.01.

Figure 3. CQ treatment rescues SN TH activity and TH density in CPu. **a**) CQ treatment did not affect the SN neuron survival (two-tailed t-test). **b**) CQ treatment did not change CPu dopamine and DOPAC levels (two-tailed t-test). **c**) Representative western blots of TH, pTH (Ser40), and actin in the SN of mice. **d**) Densitometry analysis of **c**), normalized to β-actin, suggested that SN

TH levels were unaffected by CQ treatment (two-tailed t-test). **e**) TH activity (measured by the ratio between TH expression and pTH-Ser40 expression, (50)) is significantly elevated by CQ treatment (two-tailed t-test). **f**) Representative TH-stained coronal sections of cerebrum from sham-treated (left) and CQ-treated (right) mice. Landmark (anterior commissure) was used to identify the level of coronal sectioning (bregma 0.26±0.01mm). Scale bars, 1.25 mm. **g**) CPu size is significantly greater with CQ treatment (two-tailed t-test). **h**) TH immunoreactive density in CPu is significantly elevated in CQ-treated tau knockout mice (two-tailed t-test). Dotted lines indicate our previously-reported mean values for wild-type mice at 12 months of age as a comparator (11). n=7 per treatment. Data are means ± S.E.M. *$p<0.05$.

Figure 4. CQ treatment rescues cognitive function of tau knockout mice. **a**) No differences were found in the brain wet weights of mice treated with CQ (p = 0.896, two-tailed t-test). **b**) Enlargement of the lateral ventricular area (LV) was significantly less in CQ-treated mice compared to sham-treated, accompanied by significantly greater neocortical thickness (Ctx). Corpus callosum thickness (cc) was not affected by CQ treatment (two-tailed t-test). **c**) Representative western blots of BDNF, proBDNF, and actin in the hippocampal region of mice. **d-e**) Densitometry analysis of **c**), normalized to β-actin, indicated significant elevations in levels of BDNF (**d**) and Pro-BDNF(**e**, two-tailed t-test). Dotted lines indicate our previously-reported mean values for wild-type mice at 12 months of age as a comparator (11). *$p<0.05$, versus the performance of sham-treated mice.

Figure 1

Click here to download high resolution image

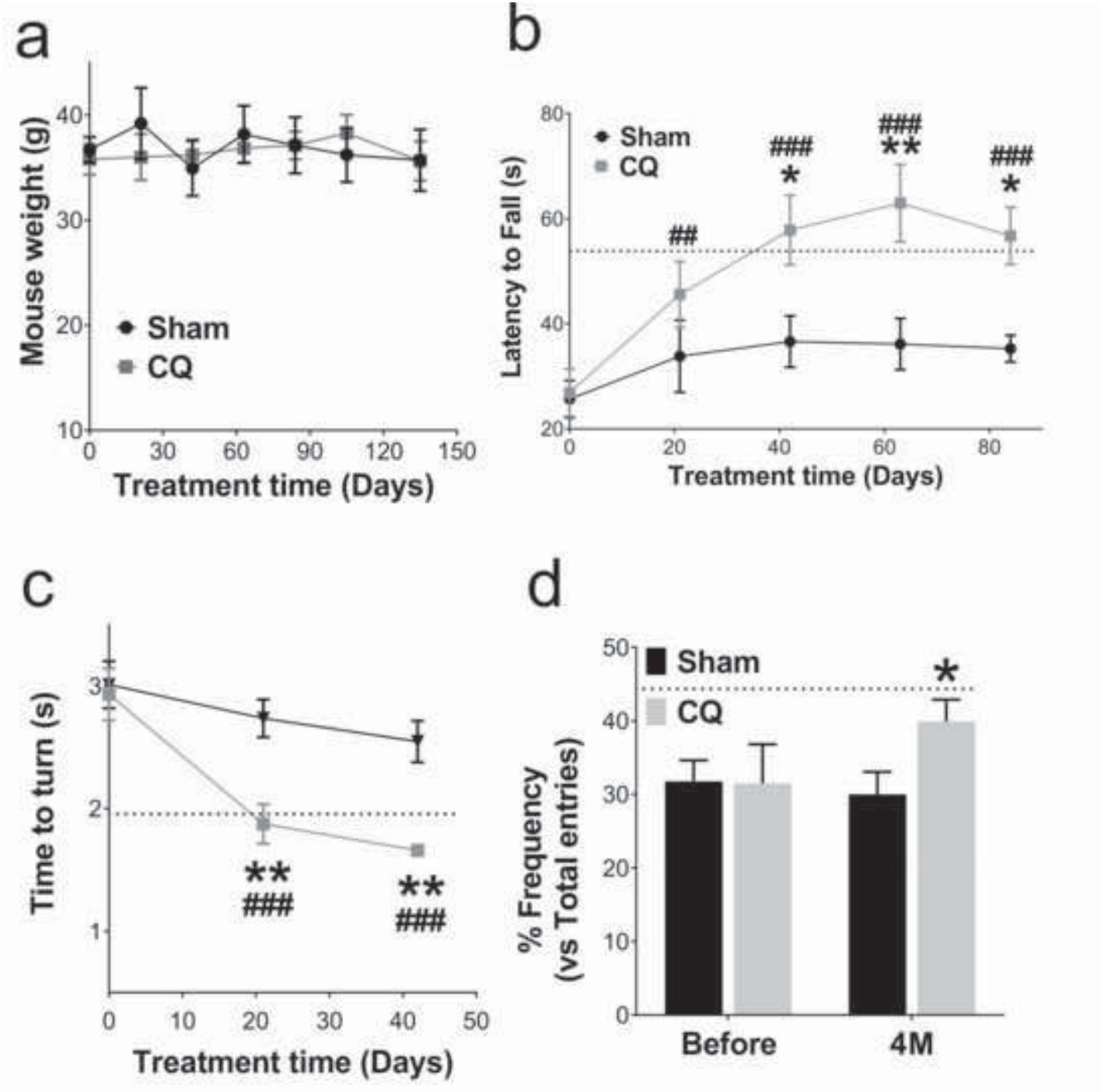

Figure 2

Click here to download high resolution image

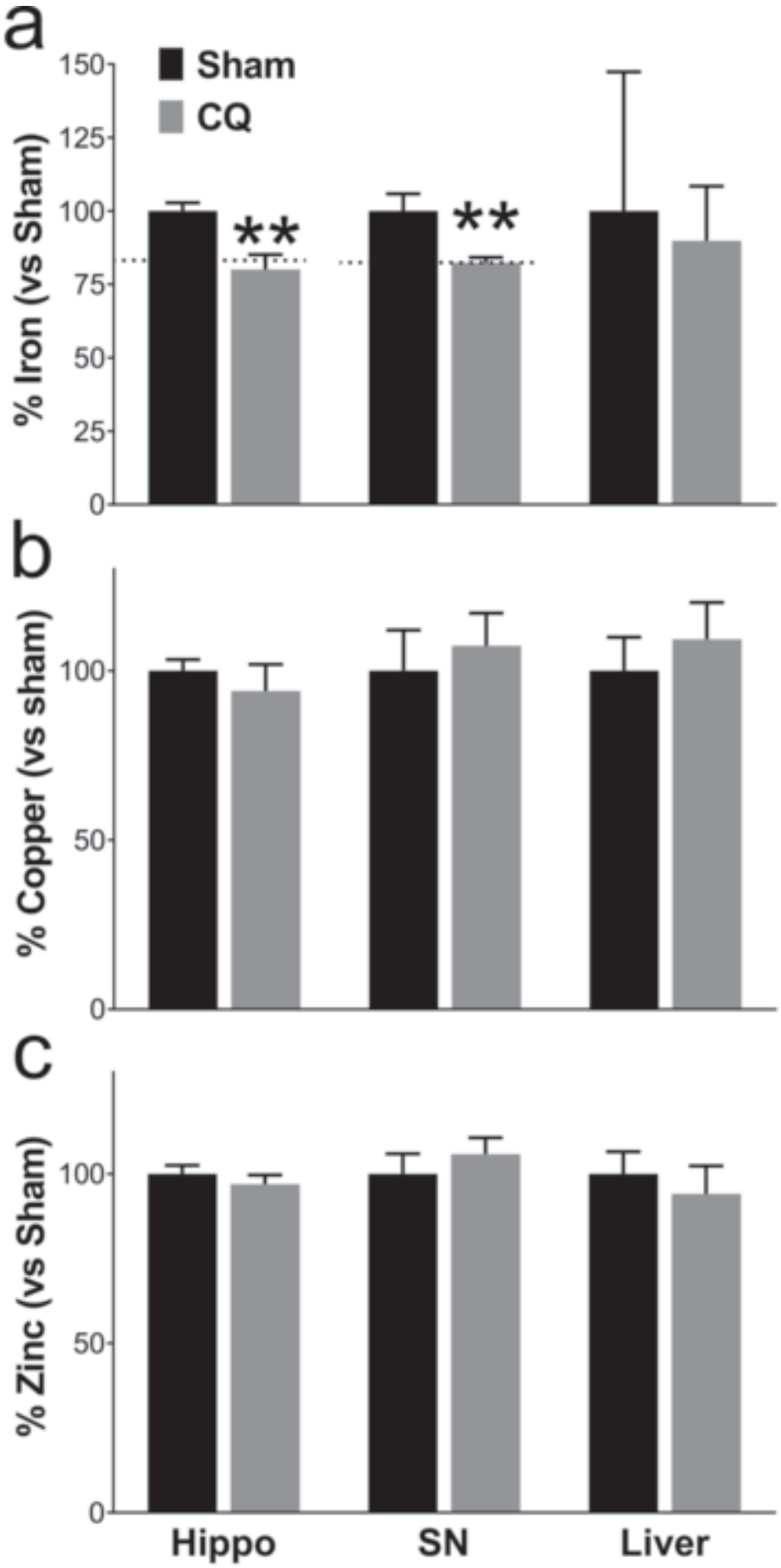

Figure 3

Click here to download high resolution image

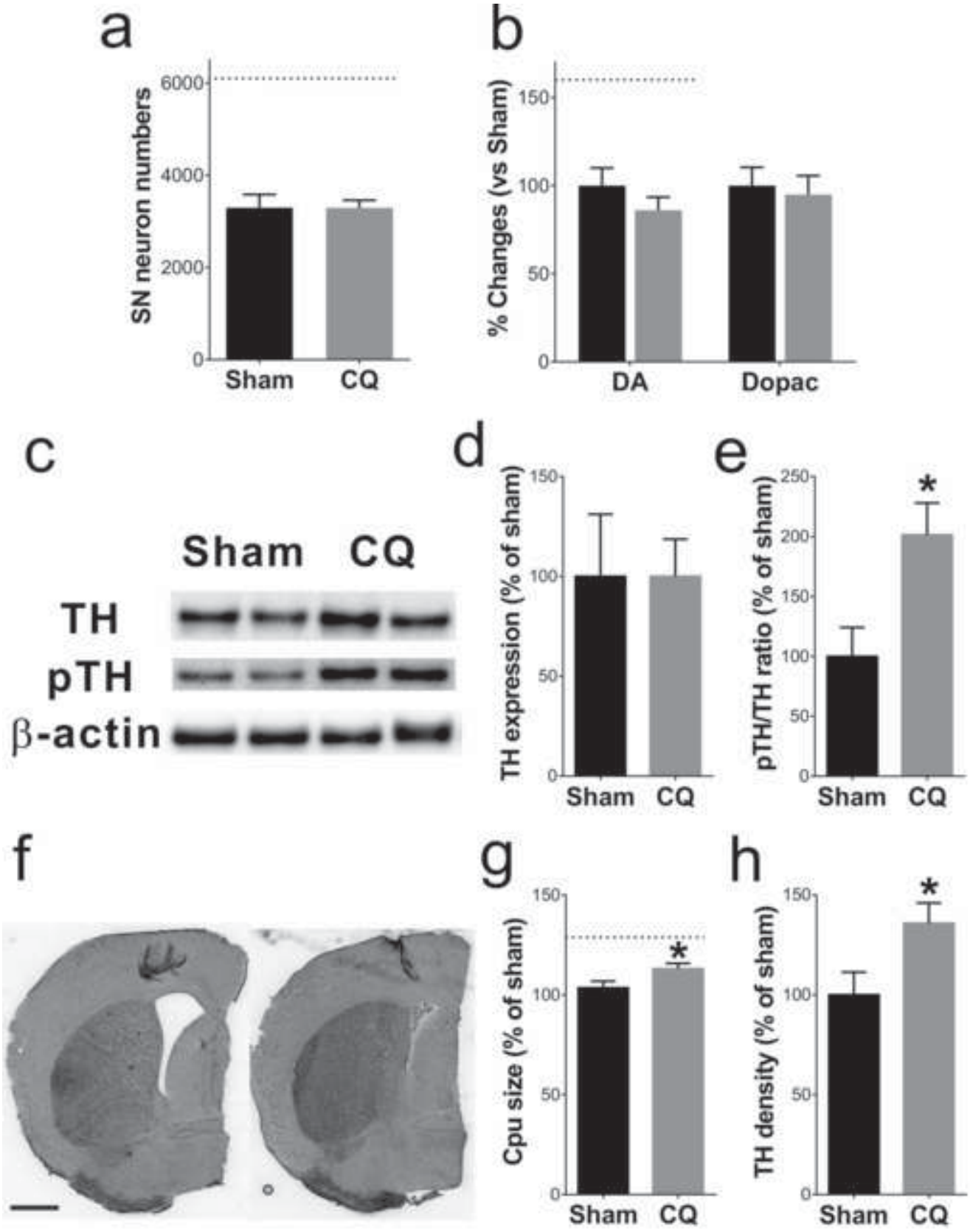

Figure 4
Click here to download high resolution image